

The Role of Nucleation Behavior in Phase-Field Simulations of the Austenite to Ferrite Transformation

M.G. MECOZZI, M. MILITZER, J. SIETSMA, and S. VAN DER ZWAAG

Three-dimensional (3-D) phase-field simulations of the austenite (γ) to ferrite (α) transformation during continuous cooling at different cooling rates were performed for an Fe-0.10C-0.49Mn (wt pct) steel, with the aim of studying the interaction between the assumed nucleation temperature range and the effective interfacial mobility when fitting transformation kinetics curves. Ferrite nuclei are assumed to form continuously over a temperature range of δT . An effective interfacial mobility is assumed with an activation energy of 140 kJ/mol and a pre-exponential factor, μ_0 . The pre-exponential factor and the nucleation temperature range are used as the only two adjustable parameters to match an experimental reference transformation curve for a particular cooling rate. The initial austenitic microstructure and the nuclei-density input data are based on experimental observations. A number of combinations of values (μ_0 , δT) are found to represent the experimental reference curve equally well when related to the accuracy of experimental measurements. The comparison between the simulated and the experimental ferrite grain-size distribution is used as an additional criterion to establish the best estimate of nucleation temperature range and interface mobility.

DOI: 10.1007/s11661-008-9517-2

© The Author(s) 2008

I. INTRODUCTION

NOTWITHSTANDING the continuous development of novel construction materials, the classical hot-rolled C-Mn steels retain their prominent position either as a very important construction material or as input material for cold-rolled steel grades. Their properties depend on their microstructure, which itself is a function of both the steel chemistry and the thermomechanical conditions imposed during rolling, subsequent controlled cooling, and coiling. Of all the processes taking place during this final production stage, the decomposition of the parent austenite phase into ferrite and pearlite remains of prime importance. Hence, it is not surprising that the decomposition of austenite has been modeled extensively, using a wide range of approaches.

In transformation models based on the classical Johnson-Mehl-Avrami-Kolmogorov (JMAK) approach,^[1-3] all attention is focused on the kinetics and all microstructural aspects are essentially ignored. However, even in the simplest JMAK model, nucleation and growth are recognized as being the two relevant and intrinsically different

processes. When fitting the JMAK equations to the experimental data, information may be obtained about both the nucleation and the growth behavior. In particular, the JMAK exponent is shown to be related to the nucleation conditions,^[4] even though only two modes of nucleation kinetics are considered: site saturation and continuous nucleation at a constant rate. In the case of site saturation, all nuclei are present and active at the start of the transformation, and their number density remains constant during the entire transformation. In the case of continuous nucleation, the number of activated nucleation sites increases at a constant rate during the transformation, with a rate of nucleus formation depending on temperature and the fraction of parent phase still present.

More refined transformation models do, however, incorporate relevant features of the parent microstructure. The simplest approach is that of Vandermeer,^[5] who considered the austenite grain as a sphere and the ferrite to nucleate uniformly along the outer surface. In this model, the final ferrite grain size is necessarily identical to the prior austenite grain size, and assuming ferrite growth to be controlled by carbon diffusion in austenite, provides a satisfactory description of austenite decomposition in most Fe-C alloys. However, more sophisticated growth parameters (*i.e.*, interface mobility, solute-drag effect) have to be introduced as adjustable parameters to describe the growth rate of ferrite in more complex alloys, including Fe-C-Mn steels.^[6-8] A geometrically more-refined model is the one in which the austenite grain is assumed to be a tetrakaidecahedron.^[9] This approach allows incorporation of the ferrite nucleation site density per austenite grain as a modeling parameter to reproduce the grain size, depending on the cooling conditions.

M.G. MECOZZI, Graduate Student, is with the Netherlands Institute for Metals Research, 2628 CD Delft, The Netherlands, and the Department of Materials Science and Engineering, Delft University of Technology. M. MILITZER, Full Professor, is with the Center for Metallurgical Process Engineering, The University of British Columbia, Vancouver, BC, Canada V6T 1Z4. J. SIETSMA, Associate Professor, is with the Department of Materials Science and Engineering, Delft University of Technology, 2628 CD Delft, The Netherlands. Contact e-mail: J.Sietsma@tudelft.nl S. VAN DER ZWAAG, Full Professor, is with the Faculty of Aerospace Engineering, Delft University of Technology, 2629 HS Delft, The Netherlands.

Manuscript submitted March 7, 2007.

Article published online April 4, 2008

In recent years, the phase field approach has emerged as one of the most powerful methods for modeling many types of microstructure-evolution processes, including the austenite decomposition.^[10–11] Based on the construction of a Landau–Ginzburg free-energy functional, the phase-field model treats a polycrystalline system, containing both bulk and boundary regions, in an integral manner. A set of continuous phase-field variables, each of them representing an individual grain of the system, are defined to have a constant value inside the grains and change continuously over a diffuse boundary of thickness η . Within this approach the initial (austenitic) microstructure is properly described, not only in two-dimensional space (2-D) but also in three-dimensional space (3-D).^[12–14] Following the formation of new (ferritic) nuclei in specific locations, depending on the cooling conditions, the microstructural evolution during the austenite to ferrite transformation is governed by the phase-field equations. The interface mobilities, interfacial energies, and the driving pressure for the transformation are parameters of the phase-field equations, and they determine the kinetics of the austenite decomposition. The driving pressure is calculated from the local carbon composition within the diffuse interface, controlled by the carbon diffusion within the austenite. Therefore, the phase-field model describes the ferrite growth *via* a mixed-mode approach, *i.e.*, both the carbon diffusion and the apparent mobility of the austenite/ferrite interface are accounted for.

The kinetics and diffusivity parameters are input data of the model, and their values have to be known for the specific material and the cooling conditions considered. The interface-energy data can be found in the literature. That is not the case for the interface mobility, which is a physically more complex parameter, which is hard to quantify with accuracy.

Also, the nucleation behavior, *i.e.*, the number of active ferrite nuclei as a function of time/temperature and their location in the initial or already partly transformed austenitic microstructure, has to be known to correctly model the austenite to ferrite transformation. The phenomenon of nucleation in solid-solid transformations has been studied extensively in the past decades,^[15–17] but an accurate link between nucleation theories and phase-field models has not been accomplished. The most important reason for this is that nucleation takes place on a length scale that is too small to incorporate in phase-field simulations of metallic microstructures. Therefore, in the phase-field model, the nucleation behavior has usually been implemented in a relatively simple manner, *i.e.*, either site saturation or a constant nucleation rate is assumed.^[13,14] Some experimental evidence does exist, however, (*i.e.*, Offerman *et al.*^[18]) that may be helpful for a better quantification of the nucleation behavior.

Not having the ambition of developing a nucleation model in its own right but to demonstrate the impact of assumptions in the nucleation conditions on the overall transformation kinetics curve and the final grain-size distribution to develop, in the present work, we use 3-D phase-field simulations, as presented in Militzer *et al.*,^[14] to investigate in a controlled and systematic manner the

effect of selected ferrite-nucleation parameters and of the effective interface-mobility value on the ferrite-growth kinetics, and the correlation between these two parameters. The simulations are focused on the austenite to ferrite transformation kinetics, as well as on the ferritic microstructure that is to develop, but the insights to be gained apply to all diffusional solid-state transformations. The ferrite nuclei are set to form at different sites, depending on the cooling conditions, while the total number of nuclei is not a “free” parameter but is derived from the ferrite grain size in the final microstructure. The nucleation temperature interval and the effective interface mobility are employed as the only two adjustable parameters to fit a representative transformation kinetics. The most realistic combination of these two is then derived by using both the experimentally determined transformation kinetics and the ferrite grain-size distribution as comparison criteria.

II. MODEL

The multiphase field model derived by Steinbach *et al.*^[10,11] is used to describe the austenite (γ) to ferrite (α) transformation kinetics. In this approach, each grain is described by an appropriate order parameter, $\phi_i(r,t)$, with $\phi_i(r,t) = 1$ if grain i is present at the location, r , and time, t , and $\phi_i(r,t) = 0$ if grain i is not present at r and t . In a transition region of width η_{ij} , $\phi_i(r,t)$ changes continuously from 0 to 1. The interfacial thickness is taken to be the same for each pair of grains in contact, *i.e.*, $\eta_{ij} = \eta$.

Each grain can have a set of attributes; in the present work, only its phase, *i.e.*, α or γ , is considered, and isotropic structural and physical properties are assumed.

Within this approach, the initial (austenitic) microstructure is described by a set of M phase-field variables, $\phi_i(r,t = 0)$, $i = 1 \dots M$, where M is the number of austenitic grains present in the initial microstructure. The formation of new (ferritic) grains, at a prescribed time, t_n , is accompanied by the addition to the system of new phase-field variables, $\phi_j(r,t)$, $j = M + 1 \dots M + P$, where P is the number of grains imposed to form at t_n . It is important to realize that the nucleation mechanism is not incorporated in the phase-field formalism; the method requires nucleation criteria to be imposed for each individual grain. In the MICRESS program, which was used for the present study, the nucleation behavior is controlled by the value of two input parameters of the model: the “shield time” and the “shield distance.” The former is the time interval after a nucleation event within which no further nucleation can take place within a volume around the nucleus that is defined by the shield distance. Thus, the shield time controls the value of the nucleation times. The shield distance is also the minimum distance between nuclei formed at the same time, thereby controlling the number and the distribution of nuclei formed at a given nucleation time.

The microstructural change occurring during the austenite to ferrite transformation is described by the time evolution of N order parameters, $\phi_i(r,t)$, if N

grains, austenitic or ferritic, are present in the system. The rate of change of each order parameter, $\phi_i(r,t)$, is given by the pair-wise interaction between neighboring grains as follows:^[14]

$$\frac{\partial \phi_i}{\partial t} = \sum_j \mu_{ij} \left(\sigma_{ij} \left[\phi_i \nabla^2 \phi_j - \phi_j \nabla^2 \phi_i + \frac{\pi^2}{2\eta^2} (\phi_i - \phi_j) \right] + \frac{\pi}{\eta} \sqrt{\phi_i \phi_j} \Delta G_{ij} \right) \quad [1]$$

Equation [1] is obtained by minimising the total free energy of the system with respect to ϕ_i , under the assumption that the free-energy density is a double obstacle function of ϕ_i . When neighboring grains have different phases, the interfacial mobilities and interfacial energies, μ_{ij} and σ_{ij} in Eq. [1], are given by the γ/α interface mobility, μ , and interface energy, σ ; ΔG_{ij} is the driving pressure for the transformation, *i.e.*, $\Delta G_{\gamma\alpha}(x^1(r,t)\dots x^n(r,t), T)$, which is a function of the temperature, T , and the local composition, $x^1(r,t)\dots x^n(r,t)$, for a system of n elements. Solute-drag effects will not be taken into account in the present study, which implies that the mobility should be seen as an effective mobility. When neighboring grains have the same phase (austenite or ferrite), μ_{ij} and σ_{ij} are the grain-boundary mobilities and energies, $\mu_{\gamma\gamma}$ or $\mu_{\alpha\alpha}$ and $\sigma_{\gamma\gamma}$ or $\sigma_{\alpha\alpha}$, respectively. In that case, ΔG_{ij} is zero, and the driving pressure for grain growth is given by the respective grain-boundary energy times the curvature term (*i.e.*, the term within the square brackets in Eq. [1]). Grain growth is assumed to be of secondary importance, due to the low value of the curvature term for both the γ/γ and α/α grain boundaries. For simplicity, grain-boundary mobilities of 5×10^{-13} m⁴/Js are assumed and the grain-boundary energies are set to a comparatively low value of 0.1 J/m² to further minimize grain growth and thus facilitating that each ferrite nucleus will lead to a ferrite grain in the final microstructures obtained in the simulations.

The present work deals with the Fe-C-Mn system and the driving pressure of the γ to α transformation depends on the local carbon and manganese concentration, as well as on the temperature, *i.e.*, $\Delta G(x^C(r,t), x^{Mn}(r,t), T)$. While in the Fe-C system, the thermodynamics are uniquely determined by the temperature and chemical composition of the system, for Fe-C-Mn, different possible constrained equilibria may be considered for manganese. In an early work,^[13] both C and Mn were assumed to redistribute in the α and γ phase. However, Mn diffusion was found to be extremely limited during the transformation times observed experimentally, even for cooling rates as low as 0.4 K/s. Thus, in subsequent simulations,^[14] it was assumed that interstitial carbon can redistribute between α and γ by long-range diffusion, and that substitutional manganese does not partition during the γ to α transformation (paraequilibrium). Satisfactory results were obtained with this assumption. Therefore, in the present work, the system is considered in the paraequilibrium limit; the driving pressure in Eq. [1] then depends on the local carbon concentration and temperature only. In the bulk of α or γ phase, as well as within the diffuse α/α or γ/γ grain-boundary area, the

local carbon concentration is given by x_α^C and x_γ^C , obtained by solving the following diffusion equations for the ferrite and austenite phase, respectively:

$$\frac{\partial x_\alpha^C}{\partial t} = \nabla \cdot (D_\alpha^C \nabla x_\alpha^C); \quad \frac{\partial x_\gamma^C}{\partial t} = \nabla \cdot (D_\gamma^C \nabla x_\gamma^C) \quad [2]$$

where D_k^C is the carbon diffusivity in phase k (α or γ). In the diffuse interface between a ferritic grain, i , and an austenitic grain, j , the α and γ phase coexist with a relative amount given by the phase-field parameters, ϕ_i and ϕ_j ; the local carbon concentration, $x^C(r,t)$, becomes a continuous variable in r through the interface, and it is built up from the carbon concentration in ferrite and austenite, x_α^C and x_γ^C , and is given by the following equation:

$$x^C(r,t) = \phi_i(r,t)x_\alpha^C(r,t) + \phi_j(r,t)x_\gamma^C(r,t) \quad [3]$$

Further, the diffusion of carbon is expressed as the sum of fluxes in the ferrite and austenite phase weighted by the phase-field parameters, ϕ_i and ϕ_j , according to the following equation:

$$\frac{\partial x^C}{\partial t} = \nabla \cdot \left[\phi_i D_\alpha^C \nabla x_\alpha^C + (1 - \phi_i) D_\gamma^C \nabla x_\gamma^C \right] \quad [4]$$

In the diffuse interface, only phase field parameters ϕ_i and ϕ_j are not zero and then $\phi_j = 1 - \phi_i$.

A distinctive feature of the model used here is that the x_α^C/x_γ^C ratio is constant within the interface, and, in the present work, is given by the following paraequilibrium ratio, $k^{C PE}$:

$$k^C = \frac{x_\alpha^C}{x_\gamma^C} = \frac{x_\alpha^{C PE}}{x_\gamma^{C PE}} = k^{C PE} \quad [5]$$

Using Eqs. [3] and [5], the carbon diffusion Eq. [4] can be written as follows:

$$\frac{\partial x^C}{\partial t} = \nabla \cdot \left\{ D^{C^*}(\phi_i) \left[\nabla x^C - \frac{x^C(k^{C PE} - 1)}{1 + \phi_i(k^{C PE} - 1)} \nabla \phi_i \right] \right\} \quad [6]$$

with

$$D^{C^*}(\phi_i) = \frac{D_\gamma^C + \phi_i(k^{C PE} D_\alpha^C - D_\gamma^C)}{1 + \phi_i(k^{C PE} - 1)} \quad [7]$$

In order to calculate $\Delta G_{\alpha\gamma}$, ThermoCalc software^[19] is used to derive the binary-phase diagram in paraequilibrium condition; to accelerate the phase-field calculations, this diagram is linearized at a reference temperature, T_R . If m_γ^{Fe-C} and m_α^{Fe-C} are the slopes of the linearized γ and α line at the reference temperature and $x_\gamma^{C R}$ and $x_\alpha^{C R}$ are the carbon contents at the reference temperature, the local equilibrium temperature, T^{eq} , corresponding to the local carbon composition, x_γ^C and x_α^C , is calculated by the following equation:

$$T^{eq} = T_R + 0.5 \left[m_{\gamma}^{\text{Fe-C}} (x_{\gamma}^{\text{C}} - x_{\gamma}^{\text{CR}}) + m_{\alpha}^{\text{Fe-C}} (x_{\alpha}^{\text{C}} - x_{\alpha}^{\text{CR}}) \right] \quad [8]$$

The factor 0.5 arises from the fact that the equilibrium temperature is averaged over the values calculated from the α and γ line.

The local undercooling is then given by the following equation:

$$\Delta T = T^{eq} - T \quad [9]$$

The driving pressure, $\Delta G_{\alpha\gamma}(x^{\text{C}}, T)$, in Eq. [1] is assumed to be proportional to the local undercooling ΔT , as given by the following equation:

$$\Delta G_{\alpha\gamma}(x^{\text{C}}, T) = \Delta S \Delta T \quad [10]$$

The value of ΔS is also evaluated using Thermocalc.

III. SIMULATION CONDITIONS

Phase-field simulations were performed to study the γ to α transformation kinetics during continuous cooling in a 3-D-simulation space. The MICRESS code^[20] was used to solve numerically the phase-field Eq. [1] and the carbon-diffusion Eq. [6]. The simulations are performed for an Fe-0.10 wt pct C-0.49 wt pct Mn steel, for which the austenite to ferrite transformation kinetics was investigated previously using the phase-field approach, both in 2-D and 3-D,^[13,14] experimental continuous-cooling transformation data are also available.^[13] Two different cooling rates of 0.4 and 10 K/s are included in this study.

Figure 1 shows the quasi-binary Fe-C phase diagram in paraequilibrium conditions, as derived by using the Thermocalc software. The assumption of paraequilibrium is probably more accurate during cooling at 10 K/s than during cooling at 0.4 K/s but is also applied here in the second case, since partitioning of manganese is very

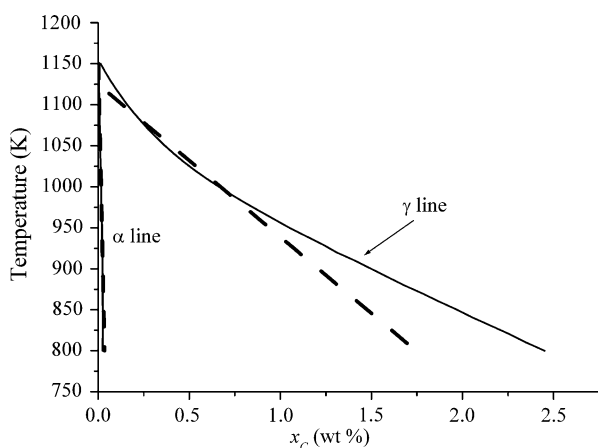


Fig. 1—Para-equilibrium Fe-C phase diagram (dashed lines are the linearized $\alpha/(\alpha + \gamma)$ and $(\alpha + \gamma)/\gamma$ boundaries).

limited as verified by previous simulations.^[13] The slopes of the $\alpha/(\alpha + \gamma)$ and $(\alpha + \gamma)/\gamma$ lines, linearized at a reference temperature, $T_R = 1073$ K, are shown in Figure 1 as dashed lines, and the carbon content in γ and α at T_R are reported in Table I. These data were employed for the driving-pressure calculation, according to Eq. (10), where the proportionality factor, ΔS , also derived using Thermocalc, is equal to 3.5×10^5 J/Km³. The equilibrium transition temperature between austenite and ferrite (A_{e3} temperature), calculated from the linearized $(\alpha + \gamma)/\gamma$ line at the nominal carbon composition of 0.1 wt pct, is equal to 1106 K.

Carbon diffusion coefficients and an austenite-ferrite interfacial energy of 0.5 J/m² were taken as described for the previous 3-D simulations.^[14]

The calculations were made for a simplified 3-D austenitic grain geometry, *i.e.*, a packing with a central tetrakaidecahedron-shaped grain, shown in Figure 2. In previous 3-D work,^[14] it was shown that the transformation kinetics are independent of the assumed initial γ microstructure if the nuclei density and distribution are the same. Table II summarizes the calculation details.

Table I. Data of the Linearized Fe-C Pseudobinary Diagram under Paraequilibrium Conditions

T_R (K)	x_{α}^{CR} (Wt Pct)	x_{γ}^{CR} (Wt Pct)	$m_{\alpha}^{\text{Fe-C}}$ (K/Wt Pct)	$m_{\gamma}^{\text{Fe-C}}$ (K/Wt Pct)
1073	0.009	0.279	-10,350	-186.2

Table II. Calculation Parameters for the Initial γ Microstructure

Domain Size (μm^3)	Number of γ Grains	d_{γ} (EQAD) (μm)	Boundary Condition
$45 \times 45 \times 45$	12	20	periodic

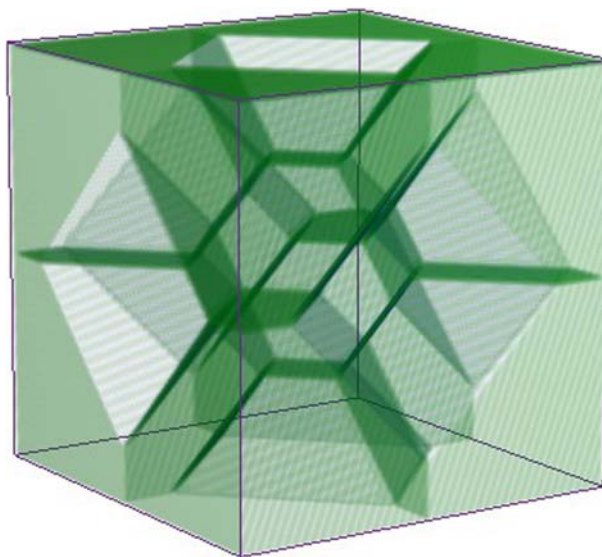


Fig. 2—Tetrakaidecahedron-shape initial austenite microstructure used in 3-D simulations.

The domain size was adjusted to have an average austenite grain size of 20 μm , equal to the value measured in metallographic cross sections of samples austenitized at 1273 K.^[13] Periodic boundary conditions are assumed in all calculations.

Time stepping, mesh size, and interface thickness were varied in initial studies, and the present values were selected to obtain convergence of the numerical simulations and, at the same time, to optimize computational effort. In detail, the mesh size, Δz , was set to 0.3 and 0.2 μm for the simulations at 0.4 and 10 K/s, respectively. In all simulations, the interface thickness, η , was set equal to four times the grid size, *i.e.*, $\eta = 4\Delta z$, which is the defacto minimum for the interface thickness in phase-field simulations.^[14]

The nucleation parameters were defined, depending on the cooling conditions. The nucleus density, ρ , is calculated from the measured ferrite grain size, d_x , using the following equation:

$$\rho = \frac{f_x}{\frac{\pi}{6}(1.2d_x)^3} \quad [11]$$

where f_x is the final ferrite fraction ($f_x = 0.9$). The average ferrite grain size in 3-D is a factor 1.2 times larger than the average equivalent area diameter of ferrite grains as measured in a 2-D metallographic section.^[21] More accurately, Eq. [11] indicates the lower limit for the ferrite nuclei density since some ferrite coarsening may occur during transformation.

Nuclei are activated in the simulations by forming a new (ferrite) grain consisting of a single volume element. At 0.4 K/s cooling rate, when the measured α grain size is approximately equal to the initial γ grain size,^[13] the number of nuclei formed in the calculation domain is approximately given by the number of austenite grains. On average, for each γ grain, one α nucleus is expected to form at a site with low activation energy, *i.e.*, at an austenite grain corner. However, the employed MICRESS code does not restrict nucleation sites to grain corners. As a result, this situation is simulated by assuming that nucleation at triple lines (TLs) is the only active nucleation mode.

At 10 K/s cooling rate, a substantial α grain refinement is observed in the final microstructure; the measured ferrite grain size is equal to 9 μm .^[11] This suggests that additional nucleation at less favorable sites, *i.e.*, the grain surfaces (GSs), must become active at lower temperatures. At the lower cooling rate, the growth of earlier formed nuclei at the grain corners (TLs in the present simulation) renders the nuclei at the grain surface inactive due to carbon enrichment in austenite and the consumption of the austenite grain-boundary area.

A nucleation study by Offerman *et al.*^[18] has shown that even during very slow cooling nucleation takes place over a certain temperature range, rather than at a single value for the undercooling. Therefore, in the present simulations, the nuclei are allowed to form during cooling continuously over a nucleation temperature range, δT , the value of which cannot, however, be derived because of the conditions being distinctly different.^[18] The influence of the chosen value for δT

will be studied in combination with the value chosen for the interface mobility, a parameter that is also not known accurately. The nucleation temperature range is controlled in MICRESS by setting the value of the input-parameter shield time, *i.e.*, the time interval after a nucleation event within which no further nucleation can take place. The number and the distribution of nuclei formed at a given temperature is controlled by the value of the shield distance, which is the radius of the zone centered in a nucleus in which nucleation is disabled.

In the simulations at 0.4 K/s, the nucleation temperature range for nucleation at TLs, δT_{TL} , is varied between 0 K (all nuclei form at a single temperature) and 24 K. In the simulation at 10 K/s, where nucleation at the GSs also occurs at lower temperatures, the total nucleation temperature range is larger compared to the case of nucleation at TLs only. A first set of simulations at 10 K/s are run by setting all nuclei to form at GSs at a constant nucleation rate within the temperature range, δT_{GS} , between 0 and 61 K. In a second set of simulations, the total nucleation temperature range is divided between two operational nucleation modes at TLs and at GSs, δT_{TL} and δT_{GS} , respectively. The number of nuclei forming at the TLs is taken to be approximately the same as for the low-cooling-rate case, and the remaining nuclei are set to form at the GSs. Table III summarizes the nucleation conditions of simulations at both cooling rates. Figure 3 shows the number of nuclei formed during cooling at 10 K/s as a function of temperature for a total-nucleation temperature range of 61 K.

Due to the impossibility of evaluating the exact ferrite nucleation start temperature from experimental observations (ferrite is only recorded after a minimum fraction of approximately 1 pct is formed), the ferrite nucleation start temperature is set equal to the temperature at which ferrite is first detected in the dilatometric tests.

The α/γ interface mobility, μ , is assumed to be temperature dependent, according to the relation $\mu(T) = \mu_0 \exp(-Q_\mu/RT)$. In the present calculations, the activation energy, Q_μ , is taken to be 140 kJ/mol, the value used by Krielaart and van der Zwaag in a study on the transformation behavior of binary Fe-Mn alloys.^[22]

For each employed cooling rate, μ_0 and δT are adjustable parameters to match a reference transformation curve, which is defined based on experimental ferrite-fraction curves derived by dilatometry.^[13] The simulated ferrite-fraction curve that fits the experimental one by setting all nuclei to form at a single temperature

Table III. The Nuclei Density and Resulting Average Ferrite Grain Size for Both Cooling Rates

Cooling Rate (K/s)	Number of Nuclei in the Domain		Nuclei Density, ρ (m^{-3})	d_x (μm)
	at the TLs	at the GSs		
0.4	15	—	1.7×10^{14}	18
10	—	118	12.9×10^{14}	9
	17	101		

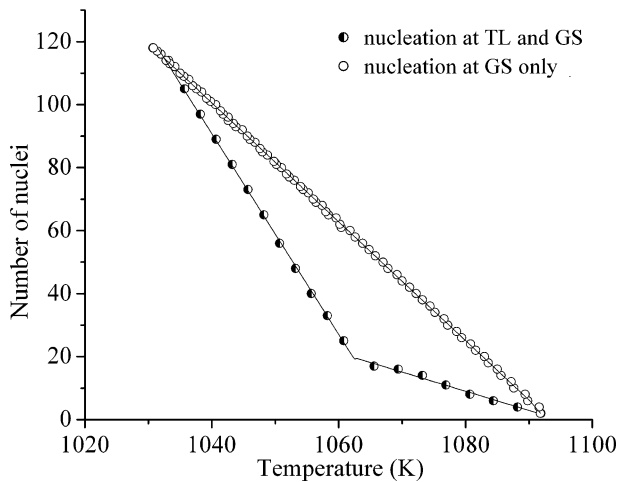


Fig. 3—Number of nuclei as a function of temperature for simulations at 10 K/s for nucleation at TLs and GSs and at GSs only, respectively, for a total-nucleation temperature interval of 61 K.

and with an adjusted mobility value is taken as the reference transformation curve.

IV. RESULTS

Figure 4 shows the simulated transformation kinetics at 0.4 K/s for a fixed value for $\mu_0 = 2.4 \times 10^{-7} \text{ m}^4 \text{ J}^{-1} \text{ s}^{-1}$ and different values of the temperature range for nucleation at TLs, δT_{TL} (lines), as well as the experimental transformation curve (symbols). The maximum nucleation temperature is estimated from the experimental ferrite-fraction curve. As expected, increasing the nucleation temperature range delays the transformation for a given mobility. For the construction of Figure 4, the interface-mobility value was selected to fit the experimental data when the nucleation temperature range is equal to zero (*i.e.*, all 15 nuclei form at 1092 K), which yielded the given value of $2.4 \times 10^{-7} \text{ m}^4 \text{ J}^{-1} \text{ s}^{-1}$. In this

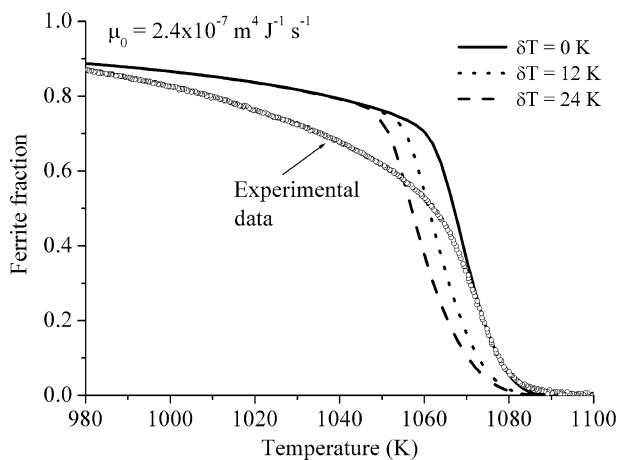


Fig. 4—Triple-line nucleation mode at 0.4 K/s (effect of nucleation temperature range, δT_{TL} , on the transformation kinetics for a given mobility).

condition, the agreement between the experimental data and the simulation is good up to a ferrite fraction of 0.5 and when the equilibrium is reached at the final stage of transformation. For the intermediate range of the ferrite fraction, the transformation rate is overestimated, which was observed and discussed previously.^[14] Figure 5 shows the transformation kinetics for a number of combinations of values ($\mu_0, \delta T_{TL}$) that fit the experimental ferrite-fraction curve comparatively well and that are all within the accuracy of the experimental curve. The increase of the interface mobility is used to compensate for the increase of the nucleation temperature range in order to obtain transformation kinetics that do not differ more from the previous curve than the typical experimental uncertainty. The transformation curves from the different simulations are not identical because the effects of nucleation behavior and interface mobility are more complex than a simple additivity suggests. Nevertheless, when comparing to experimental data, no significant difference can be identified in the experimental fraction range that can be fitted with high accuracy. Although phase-field modeling also provides microstructural information, it has been chosen in the present work to use the transformation kinetics as the principal calibration curve to determine ($\mu_0, \delta T_{TL}$) combinations. Whereas a suitable adjustment of the apparent interfacial mobility can minimise the net effect of the nucleation temperature range on the total transformation kinetics, the nucleation temperature range does have a strong effect on the microstructure formed during cooling and on the final ferrite grain size distribution. Figures 6(a) and (b) present the microstructure evolution during cooling at 0.4 K/s, with $\delta T = 0 \text{ K}$. For clarity, the initial austenite microstructure is not shown in the figure. The ferrite nuclei form at the TLs simultaneously, and each grain grows approximately isotropically. The size of all 15 grains is approximately the same, leading to a narrow grain-size distribution around a mean value of 20 μm . Figures 6(c) and (d) show the microstructure evolution during cooling at 0.4 K/s for $\delta T = 24 \text{ K}$. In this case, the size of each grain is related to its nucleation temperature.

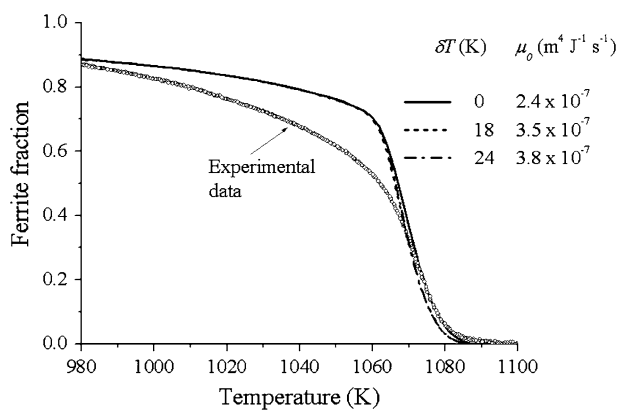


Fig. 5—Triple-line nucleation mode at 0.4 K/s (change of the pre-exponential factor of the interface mobility at different δT_{TL} to have the same transformation kinetics).

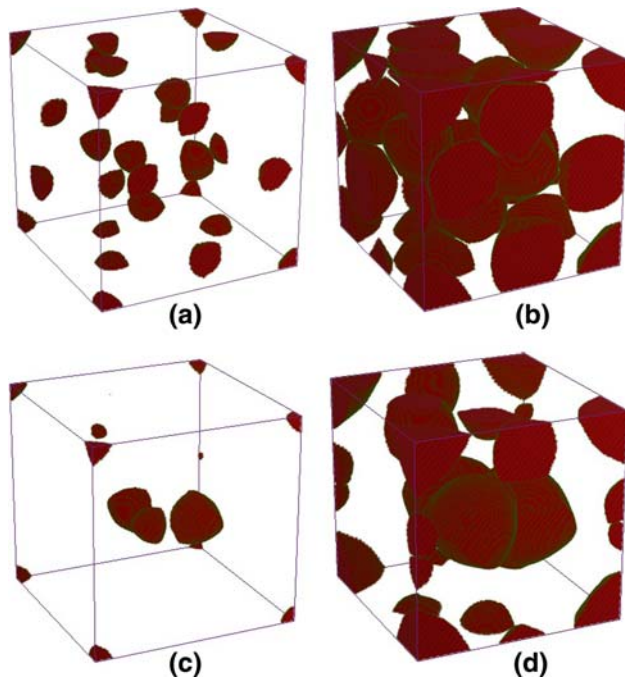


Fig. 6—Effect of δT on the simulated 3-D microstructure during cooling at 0.4 K/s for $\delta T = 0$ K (a) 1082 K and (b) 1072 K; for $\delta T = 24$ K (c) 1082 K and (d) 1072 K.

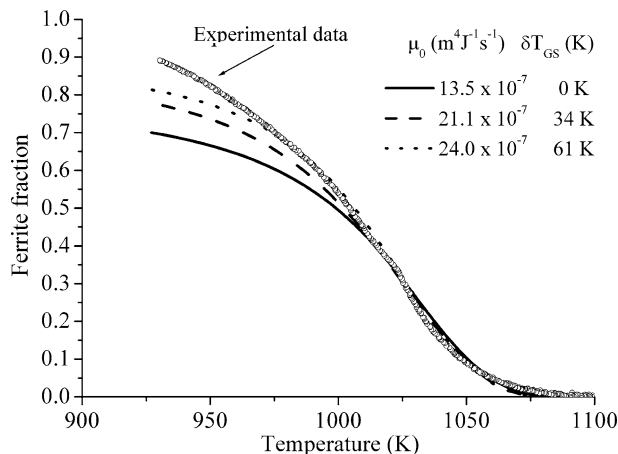


Fig. 7—Grain-surface nucleation mode at 10 K/s (change of the pre-exponential factor of the interface mobility for different values of δT_{GS} to have the same transformation kinetics).

When the last nucleus forms at 1068 K, the first grain, nucleated at 1092 K, has a size of $27 \mu\text{m}$, *i.e.*, there is a significant width in the resulting ferrite grain-size distribution. This phenomenon will be analyzed more quantitatively for the simulations at 10 K/s.

Figure 7 shows the transformation kinetics at 10 K/s in a simulation in which all 118 nuclei form at the GSs. Different combinations of μ_0 and the nucleation temperature range, δT_{GS} , are selected to fit the experimental ferrite-fraction curve, also reported in Figure 7. Unlike the situation for a cooling rate of 0.4 K/s, the necessary variation of μ_0 at 10 K/s to compensate the increase of the nucleation temperature range affects the final ferrite

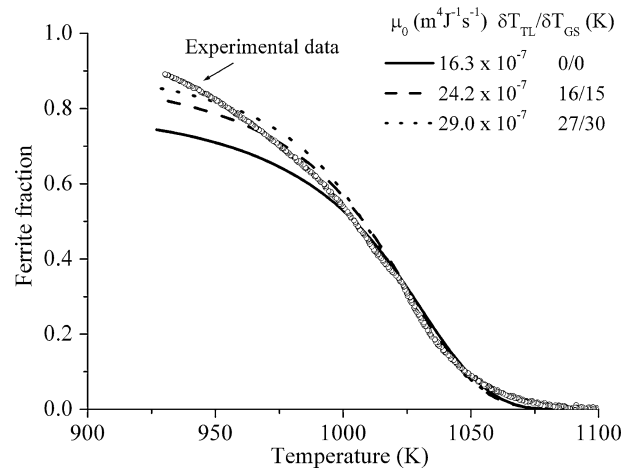


Fig. 8—Two nucleation modes at 10 K/s (change of the pre-exponential factor of the interface mobility for different values of δT_{TL} and δT_{GS} to have the same transformation kinetics).

fraction because the equilibrium cannot be reached in later transformation stages during relatively fast cooling when decreasing the interface mobility.

Figure 8 shows the transformation kinetics at 10 K/s obtained by setting both TLs and GSs as active-nucleation sites during transformation. Again, different combinations of μ_0 and the nucleation temperature ranges, δT_{TL} and δT_{GS} , are chosen to obtain the same kinetics as the reference curve. Seventeen nuclei form at the TLs, approximately the same number as for the low cooling rate case, and the remaining 101 nuclei form at the GSs. Since the nucleation temperature for a given mode is assumed to be rather insensitive to the cooling rate, the first nuclei at the TLs form again at 1092 K, similar to the low cooling rate. The remaining nuclei at the GSs form at lower temperatures. The temperature at which the first nuclei at the GSs form is set as shown in Figure 3 such that an overlap is avoided for the temperature ranges of nucleation at TLs and at GSs, respectively. When all nuclei at the TLs are set to form at a single temperature ($\delta T_{TL} = 0$ K), all nuclei at the GSs are assumed to form at an additional undercooling of 10 K.

The values of the interface mobility used to fit the reference kinetics are larger than those used in the simulations with a single nucleation mode at the GSs; this is a consequence of the initially higher nucleation rate in simulations with only nucleation at GSs (Figure 2). These results are summarized in Figure 9 where the pre-exponential factor of the interface mobility, μ_0 , is plotted as a function of the total-nucleation temperature range, δT_{total} . For a given nucleation condition, μ_0 increases with δT_{total} .

V. DISCUSSION

Early publications on phase-field modeling of the austenite to ferrite transformation showed a highly satisfactory agreement between the experimental and

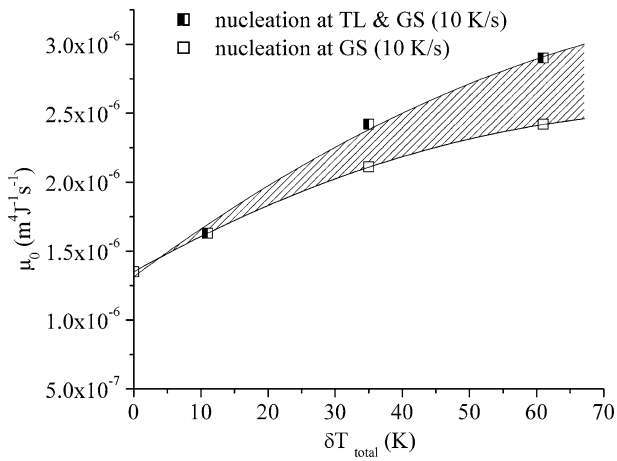


Fig. 9—Interface mobility as a function of the nucleation temperature spread to reproduce the reference transformation kinetics at each cooling rate.

simulated transformation kinetics when a suitable choice of the interface mobility was made.^[13,23] This ability was confirmed in the present work. Unlike most transformation-kinetics models, phase-field simulations are able to reproduce the morphology of the ferrite phase produced after cooling at different cooling rates.^[13] The major limit of these early studies was to restrict the modeling to a 2-D space. Recently, Militzer *et al.*^[14] reported the results of a first series of 3-D phase-field simulations of the austenite to ferrite transformation during continuous cooling. They showed that 3-D simulations not only describe the transformation kinetics better than 2-D simulations but also lead to a more realistic picture of the final microstructure.^[14] In the present work, 3-D simulations offer the further advantage of representing different types of nucleation modes better than in 2-D simulations; in 2-D simulations, all nuclei form and grow in the plane of calculation while ferrite grains that appear in 2-D cuts of a simulated 3-D microstructure may be nucleated above or below the plane of view, exactly as in 2-D sections of metallographic samples.

Another important aspect of selecting the nucleation sites is related to whether they are randomly distributed or occur in clusters. A homogeneous nuclei distribution in the calculation domain makes the entire domain to be homogeneously transformed in agreement with the experimental microstructure,^[13] while the presence of nuclei clusters and the consequently untransformed austenite region in the final microstructure can artificially reduce the final ferrite fraction (Figure 10).

One of the main results of the present investigation is that the effective interfacial mobility required to fit a given transformation curve depends strongly on the nucleation temperature range assumed: μ_0 increases with δT . The nucleation rate affects the transformation kinetics, which explains the different required mobilities at 10 K/s for nucleation at TLs and GSs, as compared to nucleation at GSs only (Figure 9). In order to combine both the nucleation temperature range and the nucleation rate in a single parameter, an average

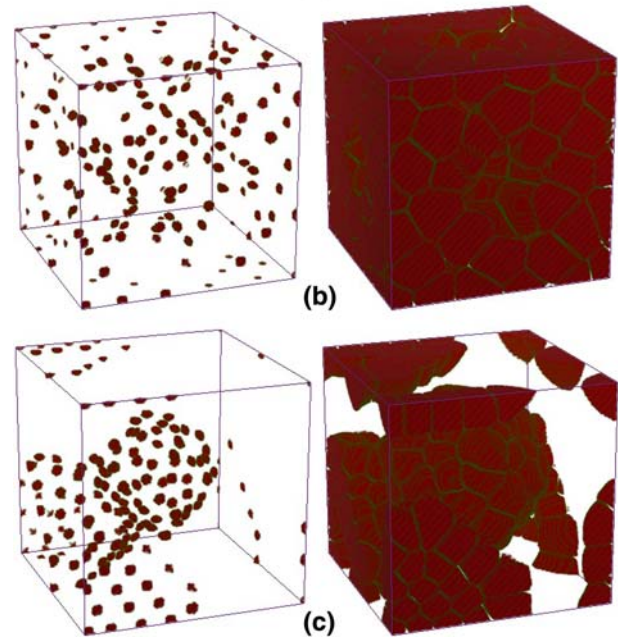
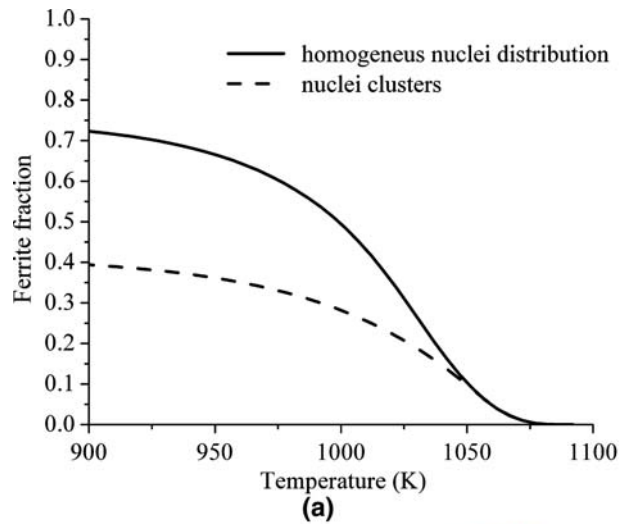


Fig. 10—Effect of nuclei distribution on the transformation kinetics: (a) microstructure developed with (b) a homogeneous nuclei distribution and (c) the presence of nuclei clusters.

nucleation temperature was calculated, weighting each nucleation temperature, T_i , with the number of nuclei, N_i , formed at this temperature, by following equation:

$$\langle T_n \rangle = \frac{\sum_i T_i N_i}{N_{\text{total}}} \quad [12]$$

Figure 11 shows μ_0 as a function of the average undercooling with respect to the maximum nucleation temperature, T_n , $\langle \Delta T_n \rangle = T_n - \langle T_n \rangle$. At 10 K/s, a single relationship was found between μ_0 and $\langle \Delta T_n \rangle$, independent of the operational nucleation modes. At 0.4 K/s, a much lower interface mobility is required to fit the transformation. This means that the pre-exponential factor for the interface mobility depends on the cooling rate. Clearly, this is in contradiction with the physical concept of the interface migration (*i.e.*, μ_0 should be

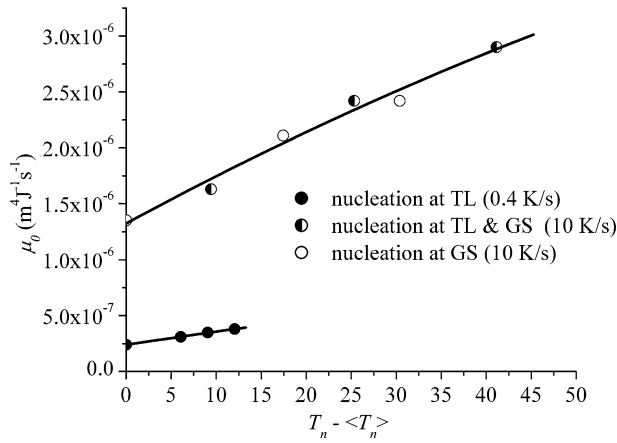


Fig. 11—Interface mobility as a function of the average undercooling with respect to the maximum nucleation temperature.

constant and independent of cooling rate), but this discrepancy has been observed in earlier studies on a different steel and also for a much wider range of cooling rates.^[24] The apparent temperature dependence of μ_0 may be related to the solute-drag effect of Mn atoms that segregate at the moving interface, as proposed by Fazeli and Militzer.^[25] In the present phase-field approach, the solute-drag term is not included in the driving-force formulation. Hence, the interface mobility, used explicitly as an adjustable parameter to fit a reference kinetics in agreement with the experimental data, does not represent the intrinsic mobility of the interface, but it is an effective parameter, which includes the solute-drag effect. If μ_0 values are normalised to the value set when all nuclei form at the same temperature, *i.e.*, $\langle \Delta T_n \rangle = 0$ K, the dependence of this normalized mobility factor on $\langle \Delta T_n \rangle$ follows the same trend for both cooling rates (Figure 12). The increase of the average nucleation undercooling, $\langle \Delta T_n \rangle$, requires a similar relative increase of the interface mobility to reproduce the target transformation kinetics. The increase of $\langle \Delta T_n \rangle$

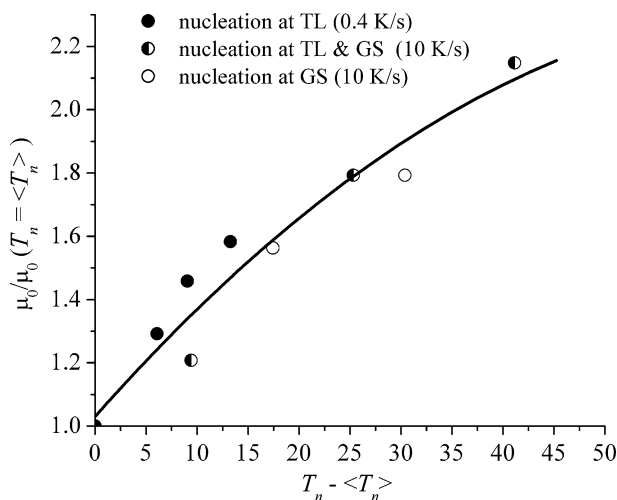


Fig. 12—Normalized interface mobility as a function of the average undercooling with respect to the maximum nucleation temperature.

from 0 to 40 K requires an increase of μ_0 by a factor of 2. Due to the difficulty in obtaining reliable nucleation data experimentally, this effect on the μ_0 value can be regarded as relatively small.

From the preceding figures and discussion, it follows that the comparison with a given reference transformation curve does not allow establishing the correct combination of μ_0 and δT unambiguously and that additional data are required. The δT range can be found directly from dedicated experiments, such as the nucleation investigation of Offerman *et al.*,^[18] or indirectly from the final ferrite grain-size distribution, as shown in this study.

In order to acquire more information on the nucleation behavior, the grain-size distribution after the transformation will also be considered. Figure 13 shows the ferrite grain-size distribution obtained in simulations at 10 K/s for various δT ranges with nucleation at GSs only and two nucleation modes, respectively. The total number of 118 ferrite grains in the final microstructure offers reasonable statistics for the evaluation of the ferrite grain-size distribution. All the grain-size distributions are fitted with a lognormal distribution defined by the following equation:^[26]

$$f(d_x) = \frac{1}{d_x S \sqrt{2\pi}} \exp \left[-\frac{(\ln d_x - M)^2}{2S^2} \right] \quad [13]$$

where M and S are the median value and standard deviation, respectively, of the variable $\ln d_x$. The mean

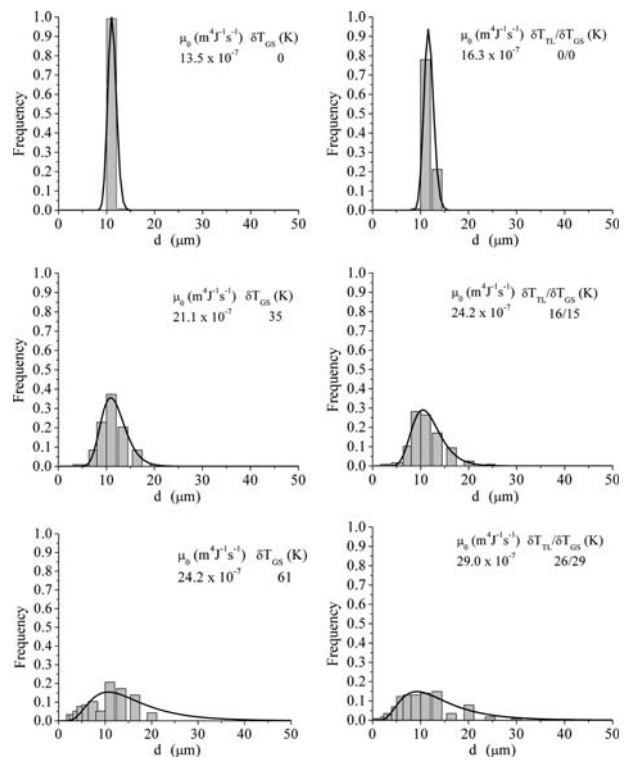


Fig. 13—Simulated ferrite grain-size distributions (bars) obtained at 10 K/s with different nucleation temperature spread for grain-surface nucleation only (left side) and triple line and grain-surface nucleation (right side) (lines show lognormal fit according to Eq. [13]).

value and the standard deviation of d_x , μ_{d_x} , and σ_{d_x} , respectively, are given by the following equations:

$$\mu_{d_x} = \int_{-\infty}^{\infty} d_x f(d_x) dd_x = e^{M+S^2/2} \quad [14]$$

$$\sigma_{d_x} = \int_{-\infty}^{\infty} (d_x - \mu_{d_x})^2 f(d_x) dd_x = \sqrt{e^{2M+S^2} (e^{S^2} - 1)} \quad [15]$$

The mean value, μ_{d_x} , is different from the peak value of the distribution, $d_x^{\text{peak}} = e^{M-S^2}$. The values μ_{d_x} and σ_{d_x} are reported for the different simulated grain-size distributions in Table IV.

The standard deviation of the distribution depends, to a first approximation, only on the total nucleation temperature range but not on the presence of a specific nucleation mode.

The bars in Figure 14 represent the experimental ferrite grain-size distribution for the sample yielding the experimental reference kinetics curve.^[13] The 2-D grain-size values as derived from metallographic measurements are converted into 3-D grain-size values, using the

Table IV. The Mean Value and the Standard Deviation of the Ferrite Grain-Size Distributions Calculated by Fitting Lognormal Distributions

	δT_{TL} (K)	δT_{GB} (K)	δT_{total} (K)	μ_{d_x} (μm)	σ_{d_x} (μm)
Nucleation at GSs	—	0	0	10.1	0.8
	—	35	35	10.2	2.3
	—	61	61	11.1	6.1
Nucleation at TLs and GSs	0	0	11	10.6	0.9
	16	15	35	9.9	2.8
	26	29	61	9.7	5.6

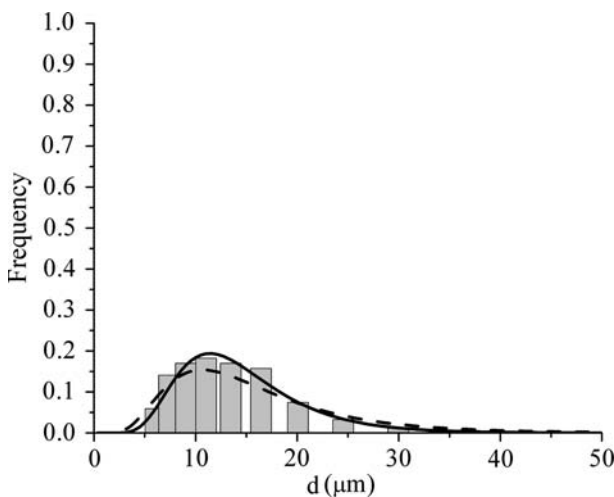


Fig. 14—Experimental ferrite grain-size distribution (bars) and lognormal fit according to Eq. [13] (solid line). The lognormal fit of the simulated grain-size distribution for a total nucleation range of 61 K is also added (dashed line).

method proposed by Matsuura and Itoh.^[27] The lognormal fit (the solid line in Figure 14) gives the values of 11.0 and 5.3 μm for the μ_{d_x} and σ_{d_x} , respectively. With these values, the simulated grain-size distribution obtained with a total temperature range of approximately 61 K fits quite well with the experimental one, as shown by the dashed line in Figure 14. This result suggests that if both nucleation at TLs and grain surface occurs for a cooling rate of 10 K/s, a nucleation temperature range of approximately 30 K for each active nucleation mode may correctly reproduce the experimental grain-size distribution.

At the lower cooling rate, nucleation occurs only at TLs with the temperature interval being comparable to that for nucleation at TLs as concluded for 10 K/s. The most realistic combination (μ_0 , δT) is then determined, giving the values of $\mu_0 = 4.2 \times 10^{-7} \text{ m}^4 \text{ J}^{-1} \text{ s}^{-1}$ and $\mu_0 = 29 \times 10^{-7} \text{ m}^4 \text{ J}^{-1} \text{ s}^{-1}$ at 0.4 and 10 K/s, respectively.

VI. CONCLUSIONS

A critical parameter study for a 3-D phase-field model of the austenite to ferrite transformation has shown that the effective interface mobility, μ , and the nucleation temperature range, δT , are strongly coupled. An increase of the δT range leads to an increase of μ to replicate a reference (experimental) kinetics. The analysis revealed an apparent cooling-rate dependence of μ that requires further investigation, *e.g.*, in terms of solute drag. However, the dependence of the relative mobility factor on the average undercooling for nucleation ($\langle \Delta T_n \rangle$) follows the same trend for both investigated cooling rates.

The experimental ferrite grain-size distribution is used to establish the most realistic combination of the values for μ and δT because the width of the ferrite grain-size distribution increases markedly with the nucleation temperature spread. The values of δT for each nucleation mode are estimated from the grain-size distribution, while the fit of the transformation kinetics is used, together with the estimated δT , to derive the effective interface mobility values for each cooling rate studied.

ACKNOWLEDGMENTS

The authors thank Access for providing the MICRESS code. The authors also thank Dr. R. Huizenga for developing the software used to visualize the evolution of 3-D microstructures.

OPEN ACCESS

This article is distributed under the terms of the Creative Commons Attribution Noncommercial License which permits any noncommercial use, distribution, and reproduction in any medium, provided the original author(s) and source are credited.

REFERENCES

1. A. Kolmogorov: *Izv. Akad. Nauk USSR Ser. Matemat.*, 1937, vol. 3, pp. 355–59.
2. W. Johnson and R. Mehl: *Trans. AIME*, 1939, vol. 135, pp. 416–58.
3. M. Avrami: *J. Chem. Phys.*, 1940, vol. 8, pp. 212–24.
4. I. Tamura, C. Ouchi, T. Tanaka, and H. Sekine: *Thermomechanical Processing of High Strength Low Alloy Steels*, Butterworth & Co. Press, London, 1988, pp. 17–48.
5. R.A. Vandermeer: *Acta Metall. Mater.*, 1990, vol. 38, pp. 2461–70.
6. Y. van Leeuwen, S.I. Vooijs, J. Sietsma, and S. van der Zwaag: *Metall. Mater. Trans. A*, 1998, vol. 29A, pp. 2925–31.
7. G.P. Krielaart and S. van der Zwaag: *Mater. Sci. Technol.*, 1998, vol. 14, pp. 10–18.
8. T.A. Kop, Y. van Leeuwen, J. Sietsma, and S. van der Zwaag: *ISIJ Int.*, 2000, vol. 40, pp. 713–18.
9. Y. van Leeuwen, T.A. Kop, J. Sietsma, and S. van der Zwaag: *J. Phys. IV*, 1999, vol. 9, pp. 401–09.
10. I. Steinbach, F. Pezzolla, B. Nestler, M. Seeßelberg, R. Prieler, G.J. Schmitz, and J.L.L. Rezende: *Physica D*, 1996, vol. 94, pp. 135–47.
11. J. Tiaden, B. Nestler, H.J. Diepers, and I. Steinbach: *Physica D*, 1998, vol. 115, pp. 73–86.
12. G. Pariser, P. Shaffnit, I. Steinbach, and W. Bleck: *Steel Res.*, 2001, vol. 72, pp. 354–60.
13. M.G. Mecozzi, J. Sietsma, S. van der Zwaag, M. Apel, P. Schaffnit, and I. Steinbach: *Metall. Mater. Trans. A*, 2005, vol. 36A, pp. 2327–40.
14. M. Militzer, M.G. Mecozzi, J. Sietsma, and S. van der Zwaag: *Acta Mater.*, 2006, vol. 54, pp. 3961–72.
15. H.I. Aaronson, H.A. Domian, and G.M. Pound: *Trans. TMS-AIME*, 1966, vol. 236, pp. 753–67.
16. H.I. Aaronson, H.A. Domian, and G.M. Pound: *Trans. TMS-AIME*, 1966, vol. 236, pp. 768–80.
17. W.C. Johnson, C.L. White, P.E. Marth, P.K. Ruf, S.M. Tuominen, K.D. Wade, K.C. Russell, and H.I. Aaronson: *Metall. Trans. A*, 1975, vol. 6A, pp. 911–19.
18. S.E. Offerman, N.H. van Dijk, J. Sietsma, S. Grigull, E.M. Lauridsen, L. Margulies, H.F. Poulsen, M.Th. Rekveldt, and S. van der Zwaag: *Science*, 2002, vol. 298, pp. 1003–05.
19. B. Sundman, B. Jansson, and J.-O. Andersson: *Calphad*, 1985, vol. 9, pp. 153–90.
20. *MICRESS® software*, ACCESS, Aachen, Germany, 2004.
21. A. Giumelli, M. Militzer, and E.B. Hambolt: *ISIJ Int.*, 1999, vol. 29, pp. 271–80.
22. G.P. Krielaart and S. van der Zwaag: *Mater. Sci. Technol.*, 1998, vol. 14, pp. 10–18.
23. Y. van Leeuwen, M. Onink, J. Sietsma, and S. van der Zwaag: *ISIJ Int.*, 2001, vol. 41, pp. 1037–46.
24. M.G. Mecozzi, J. Sietsma, and S. van der Zwaag: *Acta Mater.*, 2005, vol. 53, pp. 1431–40.
25. F. Fazeli and M. Militzer: *Metall. Mater. Trans. A*, 2005, vol. 36A, pp. 1395–1405.
26. S.K. Kurtz and F.M.A. Carpay: *J. Appl. Phys.*, 1980, vol. 51, pp. 5725–44.
27. K. Matsuura and Y. Itoh: *Mater. Trans. JIM*, 1991, vol. 32, p. 1042.